Microfluidics and Nanofluidics (2020) 24:89
https://doi.org/10.1007/s10404-020-02393-9

RESEARCH PAPER

Super-hydrophilic track for rapid directional transport of water droplets on the superhydrophobic surface

Shuyue Jiang[1] · Haifeng Zhang[1,2] · Jiamu Cao[1] · Pujun Li[1] · Keguan Song[3] · Xiaowei Liu[1,2]

Received: 15 June 2020 / Accepted: 25 September 2020 / Published online: 17 October 2020

Abstract

Directional transport of water droplet on curved track attracts considerable research interest in microfluidics. In this work, we first study the directional transport of water droplet on super-hydrophilic curved track. The water droplet can quickly move along the whole super-hydrophilic track without deviation. The speed of the water droplet on the super-hydrophilic track is 0.075 m/s. In theory, the van der Waals' force existing in the super-hydrophilic track keeps the water droplet from deviating during rapid movement. In addition, we further study the influence of track geometry and water droplet size on the transport capacity of the super-hydrophilic track. Compared with track depth, the track width has a great effect. The water droplet deviates from the track with a width of 50 µm. But the water droplet can directionally move along the super-hydrophilic track with a width of 100 µm and 150 µm without deviation. In addition, for the same super-hydrophilic track, the larger the water droplet volume, the easier it is to deviate from the track. Finally, to demonstrate the application of super-hydrophilic track on superhydrophobic surface, we performed the rapid mixing and directional collection of water droplets. This strategy is of great significance for extending it to applications such as microchannels in microfluidics, water collection systems, and others.

Keywords Super-hydrophilic track · Rapid directional transport · Superhydrophobic surface

1 Introduction

Droplet-based microfluidic systems have aroused tremendous attention owing to its remarkable advantages in miniaturized analysis filed. (Ko et al. 2014; Whitesides 2006; Stone et al. 2004) A series of applications have been reported, including biomolecular interactions, (Jeong et al. 1996; Hancock et al. 2012; Liu et al. 2010) heat transfer, (Chen et al. 2009; Li et al. 2008) and chemical reactions. (Huang et al. 2015; Tian et al. 2016) These applications are based on the mature transportation technology of water droplet. Therefore, it is crucial whether water droplets precisely move along the track or not. However, because the contact characteristics between solid phase and liquid phase, a small amount of liquid is difficult to directionally move on a solid surface. (Aussillous and Quéré 2001).

To date, several methods have been developed to actuate small water droplets on a solid surface, including electrowetting, (Gong and Kim 2008; Wheeler 2008) optoelectrowetting (OEW), (Park et al. 2010; Yu et al. 2013) dielectrophoresis, (Velev et al. 2003; Ahn et al. 2006; Millman et al. 2004) acoustic wave, (Franke et al. 2009; Wang and Zhe 2011) optical force (McGloin et al. 2008; Dholakia and Čižmár 2011) and magnetic force. (Huang et al. 2017; Long et al. 2009; Mandal et al. 2019) However, these active techniques have two disadvantages. On one hand, they lack in enough flexibility to meet diverse transport requirements of water droplet. On the other hand, chips are too complicated to fabricate for ordinary laboratories owing to integrating micromechanical/pneumatic values and electronic components into devices. Furthermore, these techniques

Electronic supplementary material The online version of this article (https://doi.org/10.1007/s10404-020-02393-9) contains supplementary material, which is available to authorized users.

✉ Haifeng Zhang
zhanghf@hit.edu.cn

✉ Keguan Song
keguan_song@163.com

[1] MEMS Center, Harbin Isnstitute of Technology, Harbin 150001, China

[2] State Key Laboratory of Urban Water Resource and Environment, Harbin Institute of Technology, Harbin 150001, China

[3] Harbin Medical University, Harbin 150001, China

require continuous power supply. To solve these problems, the special wettability surfaces (superhydrophobic surface, super-hydrophilic surface, and superoleophobic surface) attract many attentions (Ju et al. 2012; Liu et al. 2015; Comanns et al. 2015). At present, in the absence of external power source, there are three methods to achieve water droplet transportation using the special wettability surface. The first method is to use the superhydrophobic surface. Superhydrophobic surfaces with contact angles higher than 150° are demonstrated as ideal water-repellent surface (Hu et al. 2016; Schutzius et al. 2012; Dodd et al. 2016; Zheng et al. 2016). Mertaniemi et al. (2011) fabricated superhydrophobic track on superhydrophobic surface by laser cutting. They investigated the movement of water drop (20 μL) on superhydrophobic tracks (a depth of 0.3 mm and a width of 1.6 mm) under gravity. The size of water drop and track are too big to be used in droplet-based microfluidic systems. The second method is to use the superoleophobic surface to transport low surface tension liquid (Chang et al. 2011; Kobaku et al. 2012). For example, Schutzius et al. (2012) fabricated the surface tension confined (STC) open tracks for pumpless transport of liquid using large area, scalable techniques—namely spray and continuous fountain pen printing. However, the application range of this method is only for liquids with low surface tension, such as acetone, ethanol, hexadecane, etc. The third method is to use the wettability gradient surface. When a water droplet is placed on a solid surface with wettability gradient, the water droplet tends to move from low wettability surface area to high wettability area.(Chowdhury et al. 2019) The surfaces with wettability gradient are fabricated by patterning hydrophilic regions on superhydrophobic surfaces, including bioinspired coating using photolithography (You et al. 2012), breath figure method (Chen et al. 2018) or inkjet printing (Zhang et al. 2015) , micro-milling (Yang et al. 2016), atmospheric-pressure plasma jet (Wu et al. 2019). Zheng et al. (2016) fabricated the wedge-shaped super-hydrophilic area on superhydrophobic surface by cold nitrogen plasma jet. They found that water droplets would spread on the super-hydrophilic area and move toward the end of the wedge. Afterwards, Liu et al. (2019) reported a technique to induce droplets to spread from one place to anywhere required by patterning a hydrophilic region on a hydrophobic photopolymer substrate. For the wedge-shaped pattern combined with surface wettability (Ody et al. 2016; Li et al. 2017; Huang et al. 2018), there are still a series of difficulties to solve. For example, there are different structures in one surface. The multiple driving forces generated by different structures are difficult to precisely control the movement of micro-size droplets (Lin and Guo 2018). Although various researchers have performed experimental and numerical studies on the transportation of water droplet based on the special wettability surface, the different behavior of a water droplet on super-hydrophilic track is unexplored. In open-surface microfluidics, the microchannels need to meet the following conditions: (a) simple and reliable fabrication process; (b) precisely control the movement path of droplets; (c) allow droplets to quickly move along curved track without any external energy input. Therefore, an attempt is being made to achieve the directional transport of water droplets meeting the above conditions.

Here, we demonstrate a facile method to complete the directional transport of water droplets with high velocity by taking advantage of the wettability difference between super-hydrophilic and superhydrophobic surface. Water droplet is expelled from the superhydrophobic surface, but be locked in the super-hydrophilic track. We show that water droplet can move along the super-hydrophilic curved track at high velocity in experiment. We further describe the motion theory of water droplet on super-hydrophilic track in the simulation. In addition, we further study the influence of track geometry and water droplet size on the transport capacity of the super-hydrophilic track. Finally, to demonstrate the application of super-hydrophilic track on superhydrophobic surface, we performed the rapid fusion and directional collection of water droplets.

2 Material and methods

The substrate (6061 aluminum alloy) with the size of 3 cm × 3 cm × 2 mm was sanded with 1200 meshes of sandpaper, followed by ultrasonically cleaning with acetone, ethanol and deionized water for 5 min in sequence. The preparation process of the superhydrophobic track on superhydrophobic surface is as follows. First, the tracks were fabricated by laser ablation in this paper. The geometry of the superhydrophobic track is designed using Auto CAD software in Fig. 1a. The wavelength, pulse-width, repetition, and focal spot of the laser source (FPS11, Suzhou Delong Laser Co., Ltd.) were 355 nm, 25 ns, 500 kHz, and 12 μm, respectively. Second, the superhydrophobic surface is fabricated by the following steps. The first step is to fabricate the micrometer structure. The sample is immersed in a 3 M HCl solution for 12 min at room temperature (Koukoravas et al. 2016; Yu et al. 2010). The samples were cleaned with ethanol and deionized water to remove residual reactants, then dried in air. The second step is to achieve the nanostructure. The etched samples were hydrothermal synthesized in deionized water at 100 °C for 1 h. (Koukoravas et al. 2016) The final step is to achieve the superhydrophobic surface. The sample is immersed in 0.5% FAS (fluoroalkylsilane) ethanol solution for 1 h at room temperature (Yang et al. 2016). Finally, the sample is dried in 120 °C oven.

The fabrication process of super-hydrophilic track on superhydrophobic surface is divided into two steps. The first

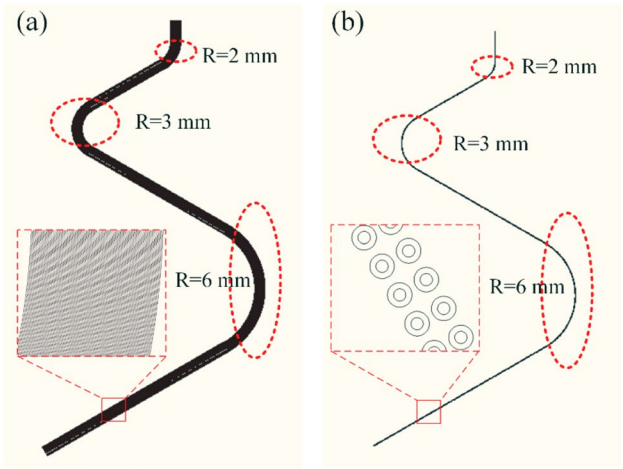

Fig. 1 CAD graphics of superhydrophobic track (**a**) and super-hydrophilic track (**b**)

step is to fabricate the superhydrophobic surface. The preparation method is the same as that of the superhydrophobic track. The second step is to fabricate the super-hydrophilic track by laser ablation. The geometry of the super-hydrophilic track is designed in Auto CAD software in Fig. 1b. The high temperature generated by focal spot removes fluorides from the superhydrophobic surface and changes the surface structure. Therefore, the surface wettability changes from superhydrophobic to super-hydrophilic.

The morphological microstructures were observed by field emission scanning electron microscope (FE-SEM, TESCAN VEGA) under a vacuum environment. Contact angles (CA) were measured by a contact angle meter system (JC2000D2A, Shanghai Zhongchen Digital Technic Apparatus Co., Ltd.) at room temperature with ultrapure water (7 μL). The movement of the water droplets was captured by a digital camera (MV-D1024E-160-CL-12, Photon focus, Switzerland).

2.1 Results and discussion

Figure 2a, d shows the topography of the sample after immersed in 0.5% FAS solution. There are two regions (I and II) on the sample, which represent different fabrication process. Region I was fabricated by the chemical etching with 3 M HCl for 12 min. Region II was prepared by thermal synthesis for 1 h on the basis of region I. In Fig. 2a and 2d, two regions (I and II) show the superhydrophobic property after immersed in 0.5% FAS (fluoroalkylsilane) ethanol solution. To confirm the influence of thermal synthesis on surface morphology, higher magnification SEM images (Fig. 2b, e) further reveal the different morphology of two regions. In Fig. 2b, prismatic structure appears on the region I after chemical etching. In the inset, the size of prismatic structure is micrometer. After thermal synthesis (region II), a layer of villous structures (boehmite) (Vitorino et al. 2015) grow on the prismatic structure (Fig. 2e). The size of villous structure is nano scale, as shown in the inset of Fig. 2e. Therefore, the villous nanostructure combined with prismatic micrometer structure can form the micronano hierarchical structure. The contact angles are shown in Fig. 2c, f. The contact angle of region II (160°) is greater than region I (153°), which means the superhydrophobic property of micronano hierarchical structure is better than micrometer structure. Aluminum ions are generated by the oxidation

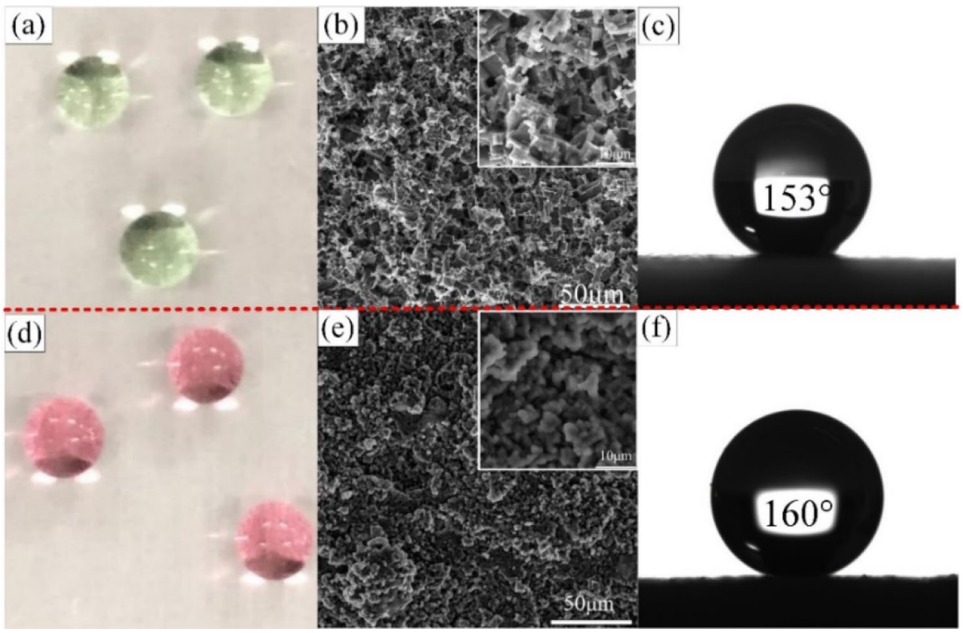

Fig. 2 Topography of the sample after immersed in 0.5% FAS solution: region I (**a**) and region II (**d**); SEM images of region I (**b**) and region II (**e**); Contact angles of region I (**c**) and region II (**f**). Insets show a high magnification view of superhydrophobic surface

of aluminum during hydrothermal synthesis, which react with OH^- (from the hydrolysis reaction of deionized water) to form $Al(OH)_3$ precipitation. When the concentration of $Al(OH)_3$ precipitation in solution reaches a certain level, $Al(OH)_3$ precipitation dehydrates to produce γ-AlOOH (the boehmite structure). Therefore, the fabricated process has the following advantages: (1) the micronano hierarchical structure has strong adhesion force to substrate owing to its growth principle; (2) the prepared surface is relatively flat, being beneficial to the fabrication of track.

The topography of super-hydrophilic track on superhydrophobic surface is shown in Fig. 3a. The depth and width of ultra-fine super-hydrophilic track are 100 μm. From the enlarged view of super-hydrophilic track (the inset of Fig. 3a), the morphology of track is round hole after laser ablation. Therefore, compared with Fig. 2e, laser ablation changed micronano hierarchical structure into hole-like micrometer structure. According to the study of Lai et al. (2010) a discrete TCL is energetically advantageous to drive a water droplet off a superhydrophobic surface, showing lower surface adhesion force. Because the discrete extent of micronano hierarchical structure is better than that of the hole-like micrometer structure, the surface adhesion force of hole-like micrometer structure is bigger than that of the micronano hierarchical structure. In addition, the high temperature generated by focal spot removes fluorides from the superhydrophobic surface. Hence, laser ablation converts the wettability of track from superhydrophobic to superhydrophilic by changing the discrete extent of microstructure and removing the fluoride. From the inset of Fig. 3a, the super-hydrophilic hole-like track can lock and store the water droplets to form the liquid layer after pre-wetting. The stationary state of a water droplet with the diameter of 3 mm on the super-hydrophilic track is showed in Fig. 3b, c. After the formation of liquid layer, van der Waals' force between a water droplet and liquid layer stretches the water droplet along the direction of the track (Fig. 3b). Perpendicular to the track, the support force from superhydrophobic surface maintains the basic shape of the water droplet (Fig. 3c), preventing the entire water droplet from completely spreading in the track.

The transportation track of water droplets includes straight lines and curves. When studying the directional transport of droplets on the track, an important indicator is whether the droplets can pass through the whole track without deviating. Regardless of special circumstances, droplets can pass through a straight track. Therefore, the straight track is not the focus of our research. Our research focuses on the curved track. Therefore, we use COMSOL software to simulate whether water droplets deviate from the track when they pass through the curved track. To observe the changes of the interface between the two phases (gas and liquid) in the simulation, the laminar flow two-phase flow level set approach is used. When water droplet moves on a curved track, the cross-section of droplet is taken as the calculate domain. The length of the air field is 16 mm and the width is 5 mm. There is a circular droplet in air. To simulate the actual situation of water droplets in air as much as possible, the upper boundary condition of the air in the model is open, and two sides are symmetrical exit boundaries. The governing equations and boundary conditions are listed in Tables 1 and 2, respectively. In governing equations, GI is the inverse

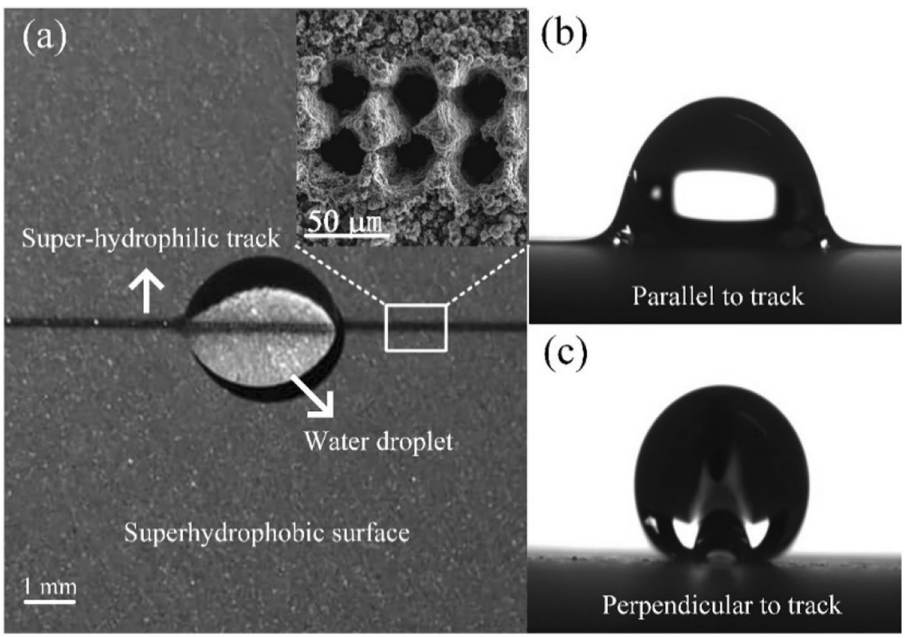

Fig. 3 **a** Topography of the super-hydrophilic track on the superhydrophobic surface; **b**, **c** Stationary state of water droplet with the diameter of 3 mm on the super-hydrophilic track from the parallel to track (**b**) and perpendicular to track (**c**). Inset shows the SEM image of the super-hydrophilic track on superhydrophobic surface.

Table 1 Governing equations in the simulation

	Governing equations
Phase initialization	$\nabla \mathrm{GI} \bullet \nabla \mathrm{GI} + \sigma_{\mathrm{w}} \mathrm{GI}(\nabla \bullet \nabla \mathrm{GI}) = (1 + 2\sigma_{\mathrm{w}})\mathrm{GI}^4$ $I_{\mathrm{w}} = \frac{1}{GI} - \frac{I_{\mathrm{ref}}}{2}$
Transient	$\rho \frac{\partial \boldsymbol{u}}{\partial t} + \rho(\boldsymbol{u} \bullet \nabla)\boldsymbol{u} = \nabla \bullet \left[-p\boldsymbol{I} + \left(\nabla \boldsymbol{u} + (\nabla \boldsymbol{u})^{\mathrm{T}}\right)\right] + \rho g + \boldsymbol{F}_{\mathrm{st}} + \boldsymbol{F}$ $\nabla \bullet \boldsymbol{u} = 0$ $\frac{\partial \phi}{\partial t} + u \cdot \nabla \phi = \gamma \nabla \cdot \left({}_{\mathrm{ls}} \nabla \phi - \phi(1-\phi) \frac{\nabla \phi}{\lvert \nabla \phi \rvert} \right)$ $\phi = \mathrm{phils}$

Table 2 Boundary conditions in the simulation

	Equations	Boundary conditions
Entrance	$\boldsymbol{n}^{\mathrm{T}}\left[-p\boldsymbol{I} + \mu\left(\nabla \boldsymbol{u} + \nabla \boldsymbol{u}^{\mathrm{T}}\right)\right]\boldsymbol{n} = -p_0$ $\boldsymbol{u} \bullet \boldsymbol{t} = 0$	$p_0 = 0$
Exit	$\left[-p\boldsymbol{I} + \mu\left(\nabla \boldsymbol{u} + \nabla \boldsymbol{u}^{T}\right)\right]\boldsymbol{n} = -p_0 \boldsymbol{n}$	$p_0 = 0$
Track wall	$\boldsymbol{n} \cdot \boldsymbol{u} = 0$ $-\nabla \cdot \boldsymbol{N}_{\phi} = 0$ $\sigma\left(\boldsymbol{n} - \boldsymbol{n}_{\mathrm{int}} \cos\left(\theta_{\mathrm{w}}\right)\right)\delta - \frac{\mu}{\beta}\boldsymbol{u} = \boldsymbol{F}_{\mathrm{fr}}$	Superhydrophobic wall $\theta_{\mathrm{w}} = pi^* 17/18$ $\beta = h$ Super-hydrophilic wall $\theta_{\mathrm{w}} = pi^* 1/18$ $\beta = h$

of the initial interface. Besides, phils represents the level set variable. The time step is range (0, 0.001, 0.06). The time step size is 0.001 s. The size of the largest and smallest unit in the grid is 0.101 and 0.00145, respectively. The curvature factor is 0.25.

When the droplet moves on a curved track, a centripetal force F of water droplet is showed in Eq. 1. v is the velocity of water droplet, and r is the radius of curvature of the track:

$$F = \int v^2 / r d_{\mathrm{m}}. \tag{1}$$

In the simulation, the relationship between the volume force f and centripetal force F is shown in Eq. 2:

$$f = \frac{F}{V} = \frac{\int v^2 / r d_{\mathrm{m}}}{\int 1/\rho d_{\mathrm{m}}} = \frac{v^2 \rho}{r}. \tag{2}$$

In the simulation, we set the radius of curvature of the curved track $r = 3$ mm. From the density of water $\rho = 1.0 \times 10^3 \mathrm{kg\ m^{-3}}$, the relationship between the volume force and the velocity of droplet is in Eq. 3:

$$f = 3.33 \times 10^5 v^2. \tag{3}$$

To study whether the droplet of the same velocity will deviate from the different track, we set the volume force of the water droplet to be the same. The volume force in the simulation is 2500 N $\mathrm{m^{-3}}$. Therefore, the velocity of water droplet is 0.086 m/s in Eq. (3).

To investigate the influence of track wettability on the movement of water droplets on curved track, we modeled the deviation of water droplets on superhydrophobic track and super-hydrophilic track by COMSOL. The simulation results are the distribution diagram of volume fraction with the time of 0.06 s. In Fig. 4a, b, the width and depth of the superhydrophobic track are 1.5 mm and 300 μm, respectively. In Fig. 4d, e, the width and depth of the super-hydrophilic track are both set to 100 μm. The stationary states of water droplets on superhydrophobic and super-hydrophilic

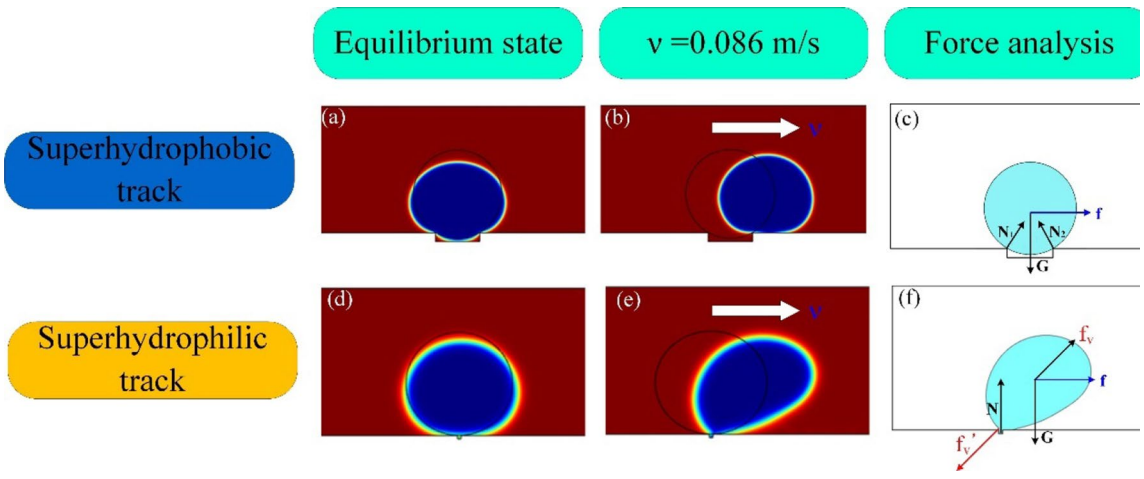

Fig. 4 Simulation results of water droplet on superhydrophobic track and super-hydrophilic track: at equilibrium state (**a**, **d**) and with the velocity of 0.086 m/s (**b**, **e**); Force analysis of the water droplet on the superhydrophobic (**c**) and super-hydrophilic track (**f**)

track are investigated in Fig. 4a, d. When the water droplet is stationary on the superhydrophobic track, the water droplet is supported only by two vertical track walls in Fig. 4a. For super-hydrophilic track, the water droplet completely penetrates the entire track owing to capillary force. Because the areas other than the super-hydrophilic track are superhydrophobic, the water droplets are still able to maintain their shape in Fig. 4d. The movement of water droplets of the same speed (0.086 m/s) on the superhydrophobic track and super-hydrophilic track is studied in Fig. 4b, e. When the water droplet passes through the superhydrophobic track with a radius of curvature of 3 mm at a speed of 0.086 m/s, the water droplet completely deviates from the track. However, for the super-hydrophilic track, although the water droplet is deformed, the water droplet is still on the track. Therefore, compared with the superhydrophobic track, water droplets with a larger velocity do not deviate from the super-hydrophilic track. To further study the reason, the force analysis of water droplet on the superhydrophobic and super-hydrophilic track is showed in Fig. 4c, f. When the water droplet moves along a curved track, the water droplet will be subjected to centrifugal force (F'). The centrifugal force causes the water droplet to derivate from its track. When the centrifugal force (F') is equal to the centripetal force (F), the water droplet moves along a curved track. When the centrifugal force (F') is greater or less than the centripetal force (F), the water droplet deviates from the track. In Fig. 4c, the supporting force (N_1 and N_2), gravity (G), and volume force (f) provide the centripetal force (F) for the water droplet to move along the superhydrophobic track. But when the velocity of water droplet is 0.086 m/s, the centripetal force (F) is not equal to the centrifugal force (F') of the water droplet. Therefore, the water droplet deviates from the superhydrophobic track. In Fig. 4f, the motion theory of super-hydrophilic track is different from that of superhydrophobic track. A layer of liquid is adsorbed in the super-hydrophilic track due to the capillary force. When the water droplet deviates from the track, the water droplet provides a large van der Waals' force f'_v (about 500 Pa) to the absorbed liquid layer. According to Newton's third law, the acting force and the reaction force are equal in magnitude and opposite. Therefore, the van der Waals' force f_v of the liquid layer to the water droplet provides the centripetal force for the water droplet to move along the curved track, as shown in Fig. 4f. For super-hydrophilic track, the centripetal force (F) is equal to the combined force of volume force (f), gravity (G), support force (N) and van der Waals' force (f_v). Compared with superhydrophobic track, the existence of f_v increases the centripetal force (F) of water droplet so that the centripetal force (F) of the droplet is equal to the centrifugal force (F'). As a result, when the droplet moves along a super-hydrophilic track at a speed of 0.085 m/s, the water droplet not deviates from the super-hydrophilic track.

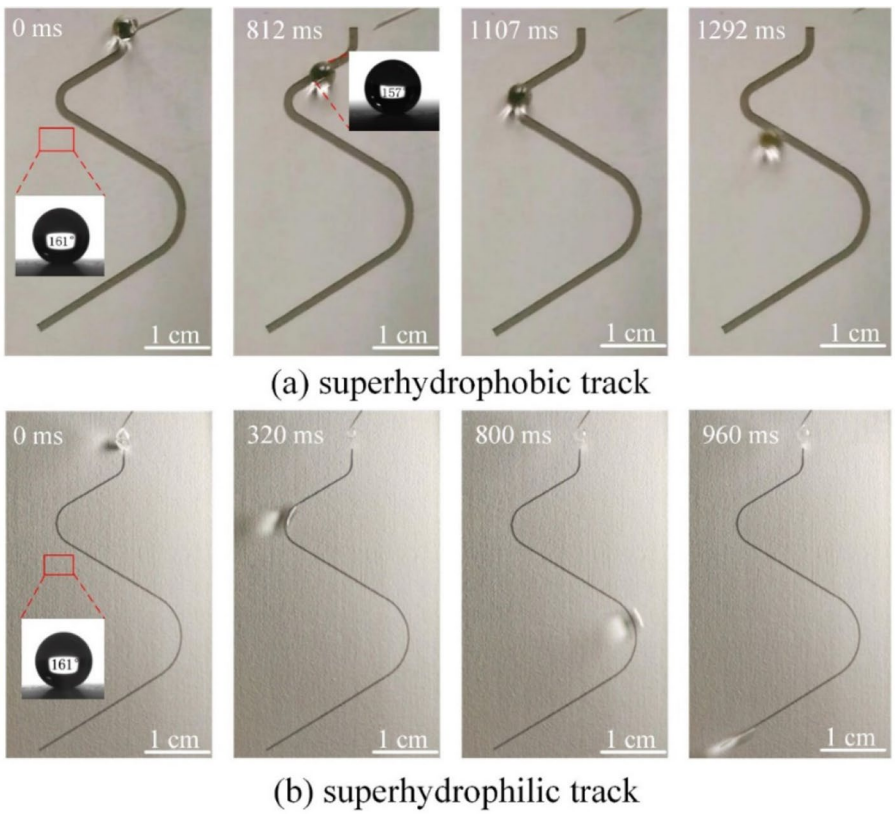

Fig. 5 A sequence of images showing the movement of water droplet on superhydrophobic (**a**) and super-hydrophilic track (**b**). Insets show contact angle of water droplet (10 µL) at different positions. See also Video S1

To study the movement of water droplets on superhydrophobic and super-hydrophilic track in experiment, the movement of water droplet is precisely recorded by the high-speed camera, as shown by a series of images in Fig. 5. The original video is available in the Supporting Information (Video S1). The track is composed of three curves with curvature radius of 2, 3 and 6 mm. The width and depth of superhydrophobic track are 1.5 mm and 300 μm, respectively. When the sample was tilted 2°, the movement of water droplet on superhydrophobic track is showed in Fig. 5a. The contact angles of water droplets (10 μL) on superhydrophobic surface and superhydrophobic track are 161° and 157° in the inset of Fig. 5a, respectively. When the water droplet has just arrived the curve with a radius of curvature of 3 mm, the water droplet deviates from the track. At the time of 1107 and 1292 ms in Fig. 5a, the water droplet cannot move along the curved track with a radius of curvature of 3 mm. It is corresponding with the simulation result (Fig. 4b). The velocity of water droplet on the superhydrophobic track is 0.01 m/s, calculated by distance divided by time. To investigate the movement of water droplet on the super-hydrophilic track, the sample was tilted to 30° in Fig. 5b. The width and depth of super-hydrophilic track are 100 μm. The water droplet can quickly pass through the whole track, corresponding with the simulation result (Fig. 4e). The velocity of water droplet on the super-hydrophilic track is about 0.075 m/s when the sample was tilted to 30°. Compared with the force analysis in the simulation (Fig. 4f), the force component of gravity (G_1) in experiment corresponds to the volume force (f) in the simulation, as shown in supplementary material Fig. S1.

To study the transport mechanism of the water droplet on superhydrophobic and super-hydrophilic track, we tilt the two samples to the same angle. The original video is available in the Supporting Information (Video S2 and S3). In Video S2, when the samples are tilted to 2°, we find that the water droplets can move on the superhydrophobic track. But when the water droplet has just arrived the curve with a radius of curvature of 3 mm, the water droplet deviates from the track. The water droplet cannot move along the track with a radius of curvature of 3 mm. However, for super-hydrophilic track, the water droplets remain immobile. When the samples are tilted to 30°, the water droplet can completely pass through the super-hydrophilic track in Video S3. However, for superhydrophobic track, the water droplet directly moves along the superhydrophobic surface of the sample, not moving along the track. The transport mechanism of the water droplet on different track is as follows. For the movement of the water droplet on the superhydrophobic track, gravity acts as the driving force. When the tilt angle (θ) becomes larger, the driving force increases. Therefore, the velocity of the water droplet increases. When the velocity of the water droplet becomes larger, the centrifugal force becomes larger. When the centrifugal force is larger than the centripetal force of the water droplet, the water droplet does not move along the track. The water droplet directly moves along the superhydrophobic surface (Video S3). For the movement of the water droplet on the super-hydrophilic track, gravity still acts as the driving force in Fig. S1b. The tilt angle (θ) becomes smaller, then the driving force decreases. When the sample is tilted to 2°, the driving force of the water droplet is not bigger than the Van der Waals' force (f_v). As a result, the water droplet does not move (Video S2). When the sample is tilted to 30° (Video S4), the water droplet begins to move because the driving force of the water droplet is greater than the resistance. From the analysis of Fig. 4 and S1 the centripetal force (F) of the water droplet on super-hydrophilic track is equal to the centrifugal force (F'). As a result, the water droplet not deviates from the super-hydrophilic track, completing the entire transport process. In summary, although the tilt angle cannot be kept the same when comparing the droplet speed on different tracks, we have found that the water droplets can be directionally transported on the super-hydrophilic track at a higher speed. Therefore, under the premise of ensuring that the water droplet can complete the directional transport on the curved track, the speed of the water droplet on the super-hydrophilic track is greater than that of the superhydrophobic track. From the above, super-hydrophilic track is more suitable for the rapid directional transport of water droplets on curved track.

The geometry of the track has a certain influence on the transport capacity of the super-hydrophilic track. The geometric dimensions of the track include the width and depth. The simulation is to study the deviation situation of water droplet when the water droplet passes through curved track. In the simulation, the volume force is 2500 $N \cdot m^{-3}$. The volume of water droplet in the simulation is 10 μL. The track in the simulation is the cross section of the track with a radius of curvature of 3 mm in experiment. The simulation results are the distribution diagrams of volume fraction. In Fig. 6, we select the time of 0, 0.04, and 0.056 s to study the effect of track geometry on transport capacity of the super-hydrophilic track. To study the track width, we simulated the deviation of the water droplets on super-hydrophilic track with the width of 50, 100 and 150 μm in Fig. 6, respectively. When simulation time is 0 s, the water droplets are in equilibrium. When the simulation time is 0.056 s, the water droplet deviates from the track with a width of 50 μm in Fig. 6c. The simulation time of 0.04 s is selected to determine whether the volume changes of the water droplets are the same in the intermediate stage. The insets of Fig. 6 are enlarged views of different tracks at different time. In Fig. 6a, d, g, the equilibrium state of water droplets on different tracks is the same. There is no water in the tracks. At the time of 0.04 s, the water droplets enter the tracks to form the liquid layer due to the super-hydrophilic

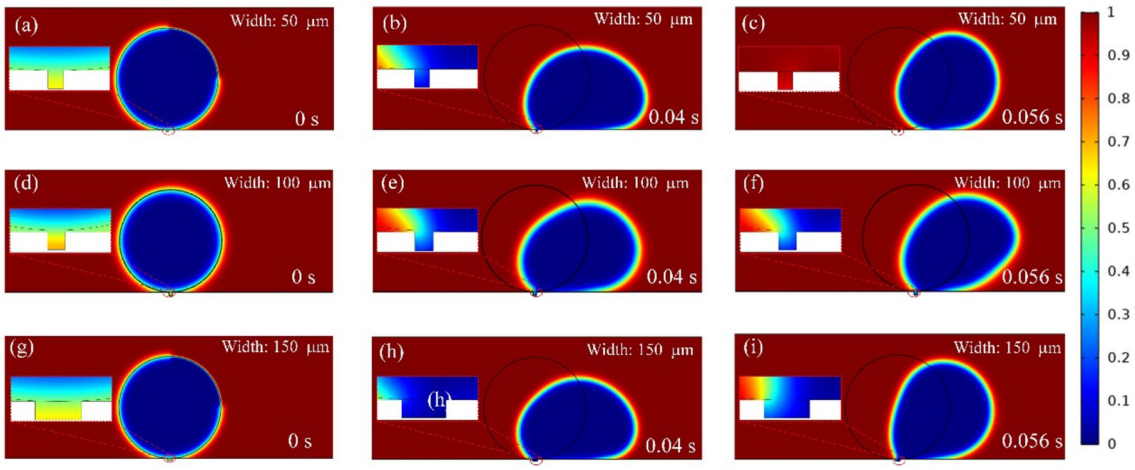

Fig. 6 Simulation results of water droplets on super-hydrophilic tracks with different widths

property of track. When the time increases to 0.056 s, the water droplet only deviated from the track with the width of 50 μm in Fig. 6c. On the other tracks (Fig. 6f, i), the water droplets are still in contact with the tracks, no deviation. The reason for this phenomenon is that the relationship between track width and liquid layer. The wider the track, the larger the contact area between water droplet and the track. As a result, the surface area of liquid layer is larger. The van der Waals' force between water droplet and the liquid layer is greater. Therefore, it is difficult for water droplets to leave the track. In addition, we also further studied the effect of track depth in the supplementary materials (Fig. S2). The width of track is 100 μm. Other simulation conditions are the same as in Fig. 6. We simulated the deviation of the water droplets on super-hydrophilic track with the depth of 20 and 100 μm in Fig. S2, respectively. We found that the water droplets did not deviate in either track. The distribution of the volume fraction at the same time is also basically the same. Therefore, the track depth has little effect on whether the water droplet deviates from the track. This is because the deepening of the track only increases the volume of the liquid layer, but has no effect on the surface area of the liquid layer. The van der Waals force between the water droplet and the liquid layer remains unchanged. Therefore, whether the water droplet deviates from the track has nothing to do with the track depth.

According to the simulation results in Fig. 6, track width affects the transport capacity of the super-hydrophilic track. To verify the accuracy of the simulation results, the movement of water droplet on tracks of different widths is precisely recorded by the high-speed camera in Fig. 7. The original video is available in the Supporting Information (Video S4 and S5). The playback speed of Video S5 is normal (30 frames per second). In Fig. 5, the water droplets quickly move along the super-hydrophilic track. Therefore, to carefully observe the movement process of the water droplets, we made the video playback speed four times slower in Video S5. The playback speed of Video S5 is 120 frames per second. In Fig. 7a, when the water droplet has just arrived the curve with a radius of curvature of 3 mm, the water droplet deviates from the track. The water droplet cannot move along the curved track with a radius of curvature of 3 mm, corresponding with the simulation results in Fig. 6a–c. When the time is 140 ms, the water droplet has left the track. When the track width increases to 100 and 150 μm, the water droplets can completely move along the entire curved track in Fig. 7b, c. The experimental results are consistent with the simulations results in Fig. 6d–i. The time for a water droplet to transport on super-hydrophilic track with a width of 100 μm is 580 ms in Fig. 7b, bigger than that of the super-hydrophilic track with the width of 150 μm (445 ms) in Fig. 7c. Therefore, for the same track, the water droplet moves faster on a track with a width of 150 μm. But because the track in Fig. 7c is too wide, the water droplet cannot maintain its shape during transportation. Therefore, in the application of microfluidic chips, a track width of 100 μm is more appropriate.

The factors that affect whether the water droplet deviates from the track are not only related to the track geometry, but also related to the size of the transported water droplet. Therefore, in our supplementary material (Fig. S3 and Video S6), we study the transportation of water droplets with the volume of 4 μL, 8 μL and 10 μL on the same super-hydrophilic track in the simulation (Fig. S3) and experiment (Video S6), respectively. In Fig. S3, 4 and 8 μL of water droplets are not off track. When the volume of the water droplet increases to 10 μL, the water droplet is off the track. In the experiment, 10 μL of water droplet deviates from the track when it passed a track with a radius of

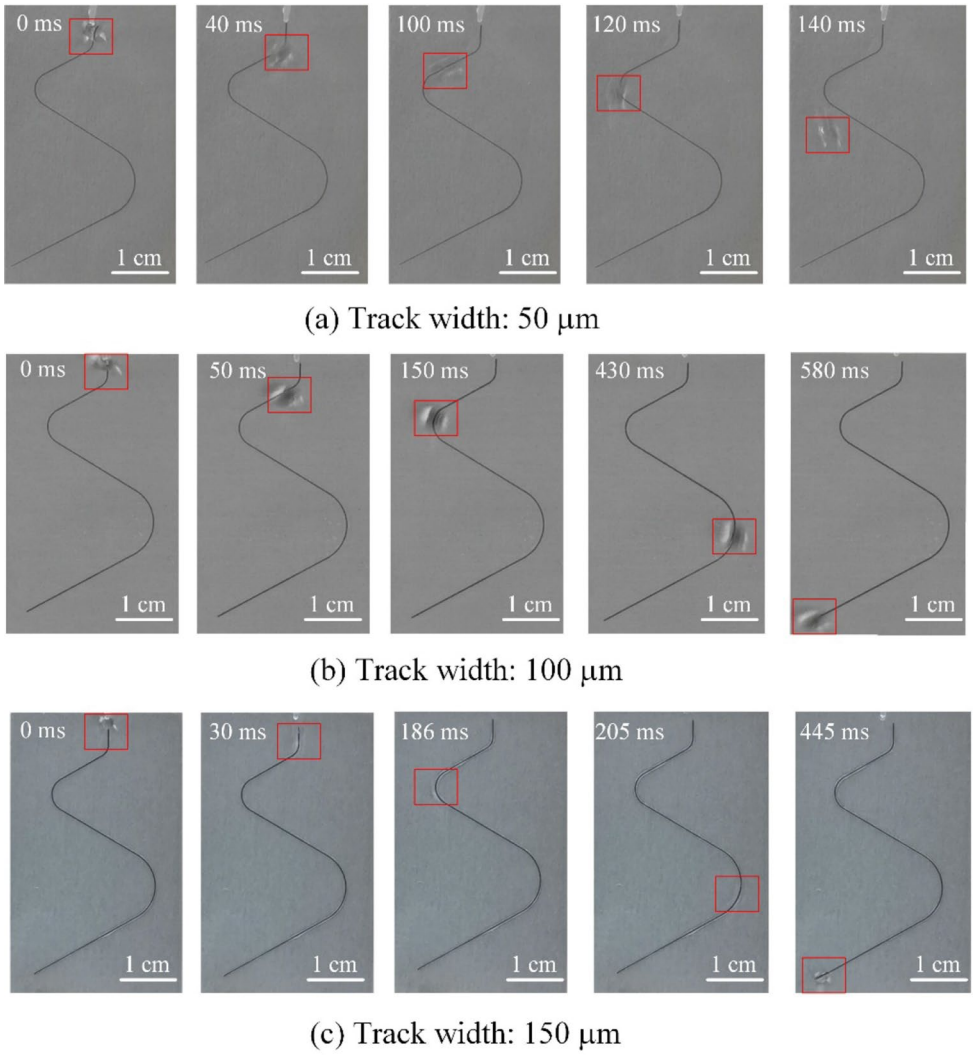

Fig. 7 A sequence of images showing the movement of water droplet on super-hydrophilic tracks with different widths: **a** 50 μm; **b** 100 μm; **c** 150 μm (see also Video S4 and S5)

curvature of 3 mm. Therefore, the experimental results are consistent with the simulation results. According to the calculation formula of centrifugal force (Guo and Chao 2013), centrifugal force is proportional to mass of water droplet. When the speed of the water droplet and the track radius are constant, the centrifugal force increases as the mass of the water droplet. Therefore, when the volume of the water droplet increases, the centrifugal force becomes larger. But the centripetal force of water droplet is same. As a result, for the 10 μL water droplet, the centrifugal force is greater than the centripetal force so that the water droplet deviates from the track.

To further prove the application of super-hydrophilic track in practice, we fabricated a junction (point *d*) of three super-hydrophilic tracks (A, B and C) on superhydrophobic surface in Fig. 8a–h. The video is available in the Supporting Information (Video S7). To observe the mixing process of the water droplets, the playback speed of video S5 was slowed down eight times. But the time marked in Fig. 8 is the actual mixing time of water droplets. In Fig. 8, the role of the super-hydrophilic tracks (A, B and C) is to quickly transport water droplets to the junction d. The morphology of the super-hydrophilic track is showed in the inset of Fig. 3a. The surface morphology of the junction d is showed in the inset of Fig. 8. Different from the hole-like morphology of the super-hydrophilic track, the junction *d* is composed of multiple concentric circles. Therefore, the super-hydrophilic area at the junction *d* is larger than that of the track, which facilitates the pinning of water droplets at the junction *d*. In Fig. 8a, b, water droplet moves along the track to the junction *d*. Owing to the super-hydrophilic property of junction *d*, water droplet is pinned at the junction *d* in Fig. 8c, d, not moving along the track. In Fig. 8e, f, the blue water droplet moves along the track to junction d and collides with the transparent droplet pinned at the junction *d*. At the moment of collision, the blue water droplet mixed with the transparent water droplet in Fig. 8g. Compared with Fig. 8f, g, the

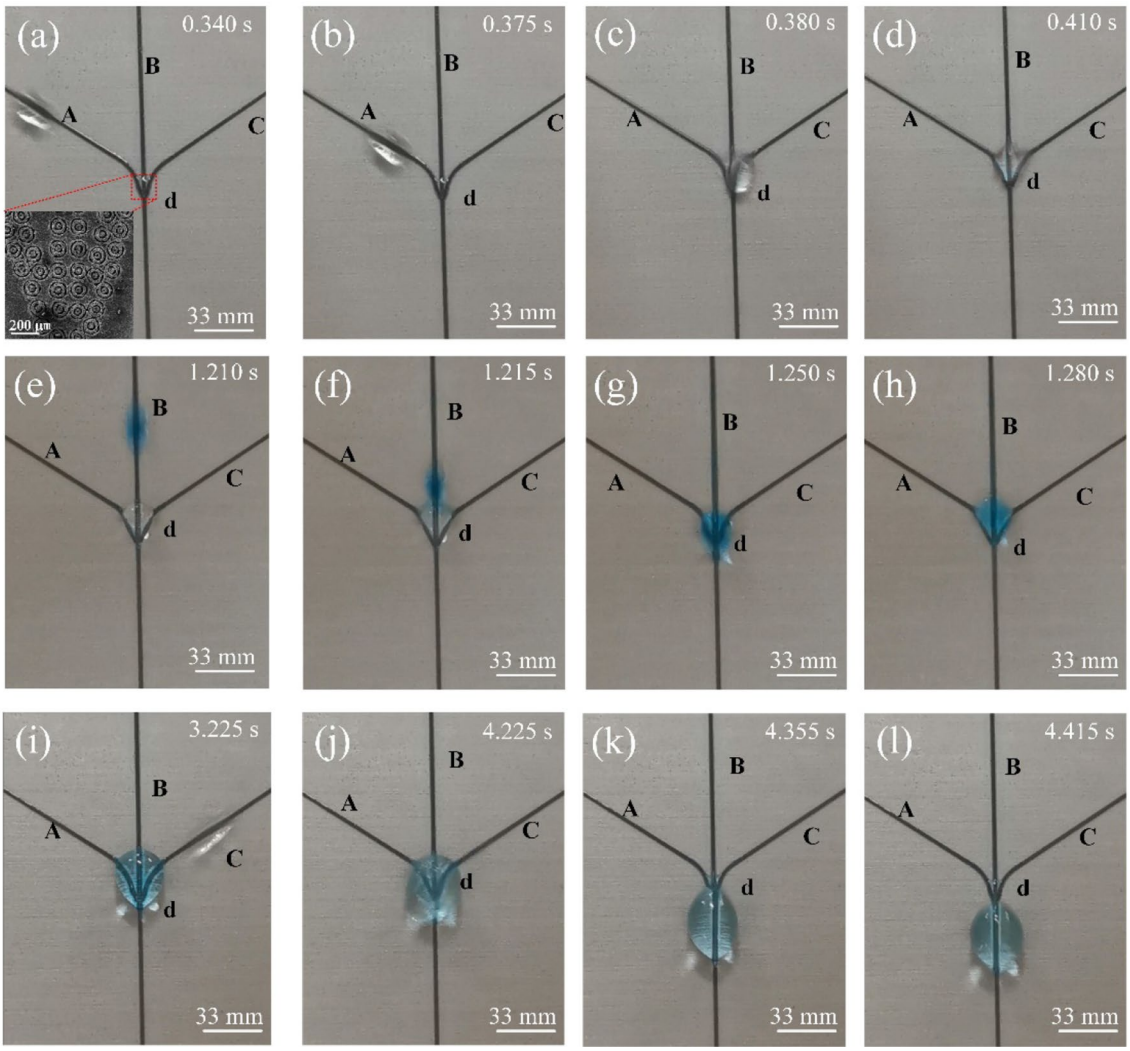

Fig. 8 A series of images showing a junction of three tracks (A, B and C) to mix the water droplets. See also Video S7

mixing time is 45 ms. Then, because the gravity of mixed water droplet is smaller than capillary force, the water droplet continues to pin at the junction d in Fig. 8h. To make the mixed water droplet move away from the junction *d*, we continue to transport the water droplets along the track C to junction *d* in Fig. 8i, j. When the gravity of the mixed water droplet is greater than capillary force, the water droplet starts to move along the track in Fig. 8k, l. Therefore, super-hydrophilic track can realize the rapid mixing of different water droplets, especially in open-surface microfluidic platforms (Morrissette et al. 2017) or mixing chip (Lai and Chung 2019).

When the number of track increases, the super-hydrophilic track can be used to collect and transport the water droplets in Fig. 9a–d. The original video is available in the Supporting Information (Video S8). On the superhydrophobic surface, the laser ablation is used to fabricate a large area of super-hydrophilic. In Fig. 9a, the super-hydrophilic surface is divided into two areas of the "capture area" and the “transport area”. The "capture area" captures water droplets owing to its super-hydrophilic property. Then the captured water droplets are transported in the “transport area” by gravity. The existence of superhydrophobic surface guarantees that the water droplets not deviate from its track during transportation. After 2 s, the water droplet gets bigger and bigger until it leaves the track in Fig. 9b–d. Further experiments confirm that this application can also be used for collecting mist liquid.

3 Conclusions

The directional transport of a water droplet on curved track is investigated in this paper. A facile method to fabricate the track on superhydrophobic surface by laser ablation is reported. Firstly, we studied the directional transport of water

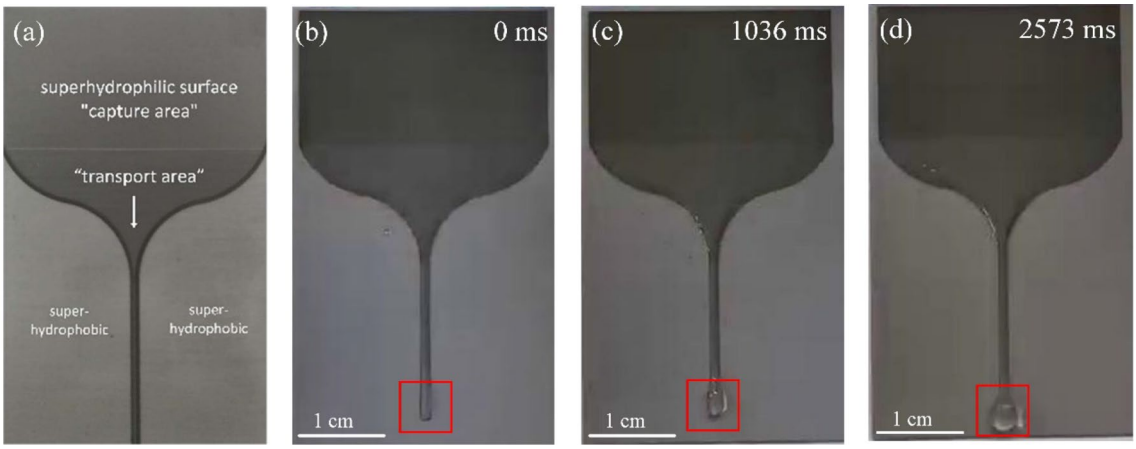

Fig. 9 **a–d** Images of water droplet collection and transport: **a** schematic diagram; **b–d** experimental diagram. See also Video S8

droplets on super-hydrophilic curved track in simulations and experiments. In simulations, we demonstrate that the motion theory of a water droplet on the super-hydrophilic track of the superhydrophobic surface. The function of superhydrophobic surface is to lift up the whole water droplet, keeping the shape of water droplet. The super-hydrophilic track can absorb the water droplets to form the uniform and stable liquid layer owing to the capillary force. The van der Waals' force between water droplets and liquid layer prevents the water droplets from moving out of track. Therefore, compared with the superhydrophobic track, the van der Waals' force existing in the super-hydrophilic track increases the centripetal force of water droplet moving along the curved track. Therefore, water droplet can quickly move along the super-hydrophilic track without deviation. As a result, the super-hydrophilic track has stronger ability to control the water droplet on the curved track (such as circle). In experiments, we show that water droplets only slowly pass through the superhydrophobic track with small radius of curvature. In contrast, water droplet can quickly pass through the whole super-hydrophilic track, including the track with large radius of curvature. Therefore, the concept of super-hydrophilic track provides a basis of the design of complex microchannels in microfluidic chips. Secondly, we further study the effect of track geometry and water droplet size on the transport ability of water droplet on super-hydrophilic track. Compared with track depth, the track width has a great effect. The water droplet deviates from the track with a width of 50 μm. But the water droplet can directionally move along the super-hydrophilic track with a width of 100 μm and 150 μm without deviation. In addition, for the same super-hydrophilic track, the larger the water droplet volume, the easier it is to deviate from the track. Finally, to demonstrate the application of super-hydrophilic track of superhydrophobic surface, we performed the rapid fusion and directional collection of water droplets. From the above, we believe that this fundamental study is of great significance for many applications such as microchannels in microfluidics, water collection systems, and others.

Acknowledgements The work is supported by National Natural Science Foundation of China (No. 61974172), Natural Science Foundation of Heilongjiang province of China (No. LH2020E059). National Basic Research Program of China (No. 2012CB934100).

References

Ahn K, Kerbage C, Hunt TP, Westervelt RM, Link DR, Weitz DA (2006) Dielectrophoretic manipulation of drops for high speed microfluidic sorting devices. Appl Phys Lett 88:024104. https://doi.org/10.1063/1.2164911

Aussillous P, Quéré D (2001) Liquid marble. Nature 411:924–927. https://doi.org/10.1038/35082026

Chang B, Sariola V, Aura S, Ras RHA, Klonner M, Lipsanen H, Zhou Q (2011) Capillary-driven self-assembly of microchips on oleophilic/oleophobic patterned surface using adhesive droplet in ambient air. Appl Phys Lett 99:034104. https://doi.org/10.1063/1.3615053

Chen Y, Zhang C, Shi M, Wu J, Peterson GP (2009) Study on flow and heat transfer characteristics of heat pipe with axial "Ω"-shaped microgrooves. Int J Heat Mass Transf 52:636–643. https://doi.org/10.1016/j.ijheatmasstransfer.2008.08.003

Chen X, Feng R, Song F, Wu JM, Luo YQ, Wang XL, Wang YZ (2018) Continuous and controlled directional water transportation on a hydrophobic/superhydrophobic patterned surface. Chem Eng J 352:722–729. https://doi.org/10.1016/j.cej.2018.07.073

Chowdhury IU, Sinha Mahapatra P, Sen AK (2019) Self-driven droplet transport: effect of wettability gradient and confinement. Phys Fluids 31:042111. https://doi.org/10.1063/1.5088562

Comanns P, Buchberger G, Buchsbaum A, Baumgartner R, Kogler A, Bauer S, Baumgartner W (2015) Directional, passive liquid transport: the Texas horned lizard as a model for a biomimetic "liquid diode." J R Soc Interface 12:20150415. https://doi.org/10.1098/rsif.2015.0415

Dholakia K, Čižmár T (2011) Shaping the future of manipulation. Nat Photonics 5:335–342. https://doi.org/10.1038/nphoton.2011.80

Dodd LE, Geraldi NR, Xu BB, McHale G, Wells GG, Cole SS, Martin J, Newton MI, Wood D (2016) Low friction water transportation on a substrate with a selective leidenfrost effect. ACS Appl Mater Interfaces 8:22658–22663. https://doi.org/10.1021/acsami.6b06738

Franke T, Abate AR, Weitz DA, Wixforth A (2009) Surface acoustic wave (saw) directed droplet flow in microfluidics for Pdms devices. Lab Chip 9:2625–2627. https://doi.org/10.1039/B906819H

Gong J, Kim CJ (2008) All-electronic droplet generation on-chip with real-time feedback control for ewod digital microfluidics. Lab Chip 8:898–906. https://doi.org/10.1039/B717417A

Guo CG, Chao CG (2013) Fabrication of isolated alloy nanoballs and nanowires using centrifugal force. Jpn J Appl Phys 44:1155–1159. https://doi.org/10.1143/JJAP.44.1155

Hancock MJ, Sekeroglu K, Demirel MC (2012) Bioinspired directional surfaces for adhesion, wetting and transport. Adv Funct Mater 22:2223–2234. https://doi.org/10.1002/adfm.201103017

Hu HB, Yu SX, Song D (2016) No-loss transportation of water droplets by patterning a desired hydrophobic path on a superhydrophobic surface. Langmuir 32:7339–7345. https://doi.org/10.1021/acs.langmuir.6b01654

Huang X, Sun Y, Soh S (2015) Stimuli-responsive surfaces for tunable and reversible control of wettability. Adv Mater 27:4062–4068. https://doi.org/10.1002/adma.201501578

Huang G, Li M, Yang Q, Li Y, Liu H, Yang H, Xu F (2017) Magnetically actuated droplet manipulation and its potential biomedical applications. ACS Appl Mater Interfaces 9:1155–1166. https://doi.org/10.1021/acsami.6b09017

Huang S, Yin SH, Chen FJ, Luo H, Tang QC, Song JL (2018) Directional transport of droplets on wettability patterns at high temperature. Appl Surf Sci 428:432–438. https://doi.org/10.1016/j.apsusc.2017.09.158

Jeong BJ, Lee JH, Lee HB (1996) Preparation and characterization of comb-like PEO gradient surfaces. J Colloid Interface Sci 178:757–763. https://doi.org/10.1006/jcis.1996.0174

Ju J, Bao H, Zheng YM, Zhao TY, Fang RC, Jiang L (2012) A multi-structural and multi-functional integrated fog collection system in cactus. Nat Commun 3:1247–1247. https://doi.org/10.1038/ncomms2253

Ko H, Lee J, Kim YJ, Lee B, Jung CH, Choi JH, Kwon OS, Shin K (2014) Active digital microfluidic paper chips with inkjet-printed patterned electrodes. Adv Mater 26:2335–2340. https://doi.org/10.1002/adma.201470096

Kobaku SPR, Kota AK, Lee DH, Mabry JM, Tuteja A (2012) Patterned superomniphobic-superomniphilic surfaces: templates for site-selective self-assembly. Angew Chem Int Ed 51:10109–10113. https://doi.org/10.1002/anie.201202823

Koukoravas TP, Ghosh A, Mahapatra PS, Ganguly R, Megaridis CM (2016) Spatially-selective cooling by liquid jet impinging orthogonally on a wettability-patterned surface. Int J Heat Mass Transf 95:142–152. https://doi.org/10.1016/j.ijheatmasstransfer.2015.11.057

Lai CC, Chung CK (2019) Numerical analysis and experiment of high-efficiency long-term PDMS open-surface mixing chip. J Micromech Microeng 29:075003. https://doi.org/10.1088/1361-6439/ab145f

Lai YK, Gao XF, Zhuang HF, Huang JY, Lin CJ, Jiang L (2010) Designing superhydrophobic porous nanostructures with tunable water adhesion. Adv Mater 21:3799–3803. https://doi.org/10.1002/adma.200900686

Li C, Wang Z, Wang P-I, Peles Y, Koratkar N, Peterson GP (2008) Nanostructured copper interfaces for enhanced boiling. Small 4:1084–1088. https://doi.org/10.1002/smll.200700991

Li C, Wu L, Yu C, Dong Z, Jiang L (2017) Peristome-mimetic curved surface for spontaneous and directional separation of micro water-in-oil drops. Angew Chem 129:13811. https://doi.org/10.1002/ange.201706665

Lin J, Guo ZG (2018) Spontaneous directional transportations of water droplets on surfaces driven by gradient structures. Nanoscale 10:13814–13831. https://doi.org/10.1039/C8NR04354J

Liu MJ, Zheng YM, Zhai J, Jiang L (2010) Bioinspired super-antiwetting interfaces with special liquid-solid adhesion. Acc Chem Res 43:368–377. https://doi.org/10.1021/ar900205g

Liu C, Xue Y, Chen Y, Zheng Y (2015) Effective directional self-gathering of drops on spine of cactus with splayed capillary arrays. Sci Rep 5:1–8. https://doi.org/10.1038/srep17757

Liu M, Yao Y, Yang YZ, Peng ZL, Chen SH (2019) Directional transport behavior of droplets on wedge-shaped functional surfaces. J Phys Chem C 123:12736–12743. https://doi.org/10.1021/acs.jpcc.9b00641

Long Z, Shetty AM, Solomon MJ, Larson RG (2009) Fundamentals of magnet-actuated droplet manipulation on an open hydrophobic surface. Lab Chip 9:1567–1575. https://doi.org/10.1039/B819818G

Mandal C, Banerjee U, Sen AK (2019) Transport of a sessile aqueous droplet over spikes of oil based ferrofluid in the presence of a magnetic field. Langmuir 35:8238–8245. https://doi.org/10.1021/acs.langmuir.9b00631

McGloin D, Burnham DR, Summers MD, Rudd D, Dewar N, Anand S (2008) Optical manipulation of airborne particles: techniques and applications. Faraday Discuss 137:335–350. https://doi.org/10.1039/B702153D

Mertaniemi H, Jokinen V, Sainiemi L, Franssila S, Marmur A, Ikkala O, Ras RHA (2011) Superhydrophobic tracks for low-friction, guided transport of water droplets. Adv Mater 23:2911–2914. https://doi.org/10.1002/adma.201100461

Millman JR, Bhatt KH, Prevo BG, Velev OD (2004) Anisotropic particle synthesis in dielectrophoretically controlled microdroplet reactors. Nat Mater 4:98–102. https://doi.org/10.1038/nmat1270

Morrissette JM, Mahapatra PS, Ghosh A, Ganguly R, Megaridis CM (2017) Rapid, self-driven liquid mixing on open-surface microfluidic platforms. Sci Rep 7:1–13. https://doi.org/10.1038/s41598-017-01725-0

Ody T, Panth M, Sommers AD (2016) Controlling the motion of ferrofluid droplets using surface tension gradients and magnetoviscous pinning. Langmuir 32:6967–6976. https://doi.org/10.1021/acs.langmuir.6b01030

Park S-Y, Teitell MA, Chiou EPY (2010) Single-sided continuous optoelectrowetting (SCOEW) for droplet manipulation with light patterns. Lab Chip 10:1655–1661. https://doi.org/10.1039/C001324B

Schutzius TM, Elsharkawy M, Tiwari MK, Megaridis CM (2012) Surface tension confined (STC) tracks for capillary-driven transport of low surface tension liquids. Lab Chip 12:5237–5242. https://doi.org/10.1039/c2lc40849j

Stone HA, Stroock AD, Ajdari A (2004) Engineering flows in small devices: microfluidics toward a lab-on-a-chip. Annu Rev Fluid Mech 36:381–411. https://doi.org/10.1146/annurev.fluid.36.050802.122124

Tian DL, Zhang N, Zheng X, Hou GL, Tian Y, Du Y, Jiang L, Dou SX (2016) Fast responsive and controllable liquid transport on a magnetic fluid/nanoarray composite interface. ACS Nano 10:6220–6226. https://doi.org/10.1021/acsnano.6b02318

Velev OD, Prevo BG, Bhatt KH (2003) On-chip manipulation of free droplets. Nature 426:515–516. https://doi.org/10.1038/426515a

Vitorino NMD, Kovalevsky AV, Abrantes JCC, Frade JR (2015) Hydrothermal synthesis of boehmite in cellular alumina monoliths for catalytic and separation applications. J Eur Ceram Soc 35:3119–3125. https://doi.org/10.1016/j.jeurceramsoc.2015.04.040

Wang Z, Zhe J (2011) Recent advances in particle and droplet manipulation for lab-on-a-chip devices based on surface acoustic waves. Lab Chip 11:1280–1285. https://doi.org/10.1039/c0lc00527d

Wheeler AR (2008) Chemistry: putting electrowetting to work. Science 322:539–540. https://doi.org/10.1126/science.1165719

Whitesides GM (2006) The origins and the future of microfluidics. Nature 442:368–373. https://doi.org/10.1038/nature05058

Wu ST, Huang CY, Weng CC, Chang CC, Li BR, Hsu CS (2019) Rapid prototyping of an open-surface microfluidic platform using wettability-patterned surfaces prepared by an atmospheric-pressure plasma jet. ACS Omega 4:16292–16299. https://doi.org/10.1021/acsomega.9b01317

Yang XL, Liu X, Lu Y, Song JL, Huang S, Zhou SN, Jin ZJ, Xu WJ (2016) Controllable water adhesion and anisotropic sliding on patterned superhydrophobic surface for droplet manipulation. J Phys Chem C 120:7233–7240. https://doi.org/10.1021/acs.jpcc.6b02067

You I, Kang SM, Lee S, Cho YO, Kim JB, Lee SB, Nam YS, Lee H (2012) Polydopamine microfluidic system toward a two-dimensional, gravity-driven mixing device. Angew Chem Int Ed 51:6126–6130. https://doi.org/10.1002/anie.201200329

Yu ZJ, Yu YF, Li YF, Song SP, Huo SB, Han XY (2010) Preparation and characterization of super-hydrophobic surfaces on aluminum and stainless steel substrates. Surf Rev Lett 17:375–381. https://doi.org/10.1142/S0218625X10014132

Yu TM, Yang SM, Fu CY, Liu MH, Hsu L, Chang HY, Liu CH (2013) Integration of organic opto-electrowetting and poly(ethylene) glycol diacrylate (PEGDA) microfluidics for droplets manipulation. Sens Actuators B Chem 180:35–42. https://doi.org/10.1016/j.snb.2011.12.059

Zhang LB, Wu JB, Hedhili M, Yang XL, Wang P (2015) Inkjet printing for direct micropatterning of a superhydrophobic surface: toward biomimetic fog harvesting surfaces. J Mater Chem A 3:2844–2852. https://doi.org/10.1039/c4ta05862c

Zheng HX, Huang S, Liu JY (2016) Vein-like directional transport platform of water on open aluminiuml substrate. Micro Nano Lett 11:269–272. https://doi.org/10.1049/mnl.2015.0588